

Direct Dynamics with Applications to Photochemical Reactivity

*Submitted in partial fulfilment of the requirements for the degree of PhD.,
University of London.*

by

Barry Robert Smith

January 1998

Department of Chemistry
King's College London

Abstract

Traditional techniques for computing classical trajectories are problematic when dealing with many degrees of freedom. One might usually expect to map-out the entire potential energy surface (PES) before starting the calculation. *Direct dynamics* is a method which overcomes this problem by removing the need to compute the PES explicitly.

When studying photochemical systems one encounters a fundamental problem: the detailed bond-breaking / bond-making processes which occur in these reactions must be modelled using some form of quantum-mechanical potential surface. An efficient solution is to employ a *hybrid* potential, which utilises a combination of quantum and classical theory to generate the electronic structure data required for a trajectory.

This thesis describes a method which combines direct dynamics with a hybrid potential — MM-VB (molecular mechanics with valence bond) — making it possible to study the dynamics of quite large organic photochemical systems without neglecting any degrees of freedom at all. *Conical intersections* (surface crossings) play a fundamental role in photochemical mechanisms. To simulate transfer through an intersection, a trajectory-surface-hopping (TSH) algorithm is used.

Our aim is to understand the factors which control photoproduct distribution, and to examine general dynamic effects caused by the reaction path and surface topology. The first four reactions we have studied involve the photochemistry of azulene, benzene, cyclohexadiene/hexatriene and all-trans octatetraene, respectively. Full dynamics involving all degrees of freedom have never before been computed for any of these systems. The fifth application chapter documents some interesting soliton-type dynamics which we predict can occur in linear polyenes, via a conical intersection mechanism. The final project, a host-guest study using a cyclodextrin cavity, demonstrates the effectiveness of MM-VB direct dynamics for studying large systems.

Contents

List of Figures	8
List of Tables	13
List of Acronyms	13
Acknowledgements	14
Chapter 1 Introduction	15-33
1.1 Modelling Photochemical Reactivity	15
1.2 The Born-Oppenheimer Approximation	23
1.3 The Potential Energy Surface and it's Interpretation	25
1.3.1 General Concepts	25
1.3.2 Conical Intersections	28
Chapter 2 Direct Dynamics and Trajectory Surface Hopping	34-76
2.1 Direct Dynamics	34
2.1.1 Introduction	34
2.1.2 Derivation of Direct Dynamics Equations	38
a) The classical Lagrange equations of motion	38
b) The kinetic energy and the G-Matrix	40
c) The local quadratic approximation to the PES	41
d) The new equations of motion in terms of internal coordinates	42
e) Decoupling the classical equations of motion	43
f) New expressions for the kinetic energy and momentum	45
g) Analytic solutions to the decoupled equations of motion	46
2.1.3 The Trust Region	48
2.1.4 Criticisms of Direct Dynamics	49
2.2 Trajectory Surface Hopping	51
2.2.1 Introduction	51
2.2.2 Semi-Classical Treatment	52
2.2.3 Interpretation of the Semi-classical Equations	56
2.2.4 Deciding when to Hop	57
2.2.5 Velocity Rescaling and Energy Redistribution at the Surface Hop	62
2.2.6 'Ants' and 'Anteaters'	65
2.2.7 Initial Conditions for the Trajectories	66

(Chapter 2 continued)

2.3 Computational Details	69
2.3.1 Molecular Dynamics on Parallel Computers	70
2.3.2 Flowcharts for the Dynamics Code	71
2.3.3 Analysis of the Trajectory Results	74

Chapter 3 The Molecular Mechanics with Valence Bond (MM-VB) Hybrid Potential 77-100

3.1 Introduction	77
3.2 The Molecular Mechanics Part of MM-VB	79
3.3 The Valence Bond Model	80
3.3.1 Heitler-London Treatment of H ₂	80
3.3.2 A Parametrised VB Approach: the LEPS function	83
3.4 The Valence Bond Part of MM-VB	87
3.4.1 The Heisenberg Hamiltonian	87
3.4.2 Parametrisation in MM-VB	89
3.4.3 MM-VB Treatment of Multi-Centre Reactions	91
3.4.4 Summary and Other Details	92
3.5 Practical Aspects of Running an MM-VB Dynamics Calculation	94
3.6 Conclusion	100

Chapter 4 Azulene: Ultrafast Decay Dynamics via a Tipped Conical Intersection 101-119

4.1 Introduction	101
4.2 Computational Details	103
4.3 Results and Discussion	103
4.3.1 Topology of the S ₁ and S ₀ Potential Energy Surfaces	103
4.3.2 Dynamics of Trajectories Constrained to S ₁	107
4.3.3 Dynamics of Surface Hopping Trajectories	110
4.3.4 Testing the Accuracy of the Trajectory Code	113
4.4 Conclusion	117
Appendix 4 Supplementary Data	118

Chapter 5 ‘Classical Wavepacket’ Dynamics through a Conical Intersection: Application to the S₁/S₀ Photochemistry of Benzene	120-140
5.1 Introduction	120
5.2 Computational Details	121
5.3 Results and Discussion	123
5.3.1 Topology of the S ₁ and S ₀ Potential Energy Surfaces	123
5.3.2 Classical Wavepacket Results	128
5.4 Conclusion	137
Appendix 5 Supplementary Data	138
Chapter 6 The Mechanism of Product-Formation in the Cyclohexadiene/Hexatriene Photochemical Interconversion	141-161
6.1 Introduction	141
6.2 Initial Relaxation Directions from a Conical Intersection	144
6.3 Computational Details	147
6.4 Results and Discussion	150
6.4.1 The Conical Intersection and Ground State Relaxation Paths	150
6.4.2 Dynamics Simulations	155
6.5 Conclusion	160
Appendix 6 Supplementary Data	161
Chapter 7 Photochemical Isomerisation of Octatetraene	162-206
7.1 Introduction	162
7.2 Computational Details	166
7.3 Results and Discussion	167
7.3.1 MM-VB Optimised Structures.	167
7.3.2 Characterisation of the Conical Intersection.	171
7.3.3 Excited State Dynamics in the Region of the Two Transition Structures.	174
7.3.4 Comparison with <i>ab initio</i> Data.	177
7.3.5 How Do Trajectories Reach the CI ?	180
7.3.6 Visualising the Potential Energy Surfaces	184

(Chapter 7 continued)

7.3.7 Relaxation Paths from the CI.	188
7.3.8 Results of ‘Classical Wavepackets’ Through the Conical Intersection.	189
7.4 Conclusion	200
Appendix 7 Supplementary Data	202

**Chapter 8 Decay Dynamics of Polyenes: Solitons and
Electronic Recoupling Mechanisms** **207-252**

8.1 Introduction: the soliton in chemical systems	207
8.2 Background and Theory	209
8.2.1 Mechanism For Formation of Solitons in Polymers and Polyenes	209
8.2.2 ‘Normal’ and ‘Reverse’ Electronic Recoupling via a Conical Intersection	213
8.3 Results and Discussion	217
8.3.1 Stable Reverse Recoupling Regions for Octatetraene	217
8.3.2 Stable Reverse Recoupling Regions for Hexatriene and Dodecahexaene	219
8.3.3 <i>Ab Initio</i> Evidence for Reverse Recoupling in Hexatriene	222
8.3.4 Detailed MM-VB Study of the Relaxation Channels from the Dodecahexaene Conical Intersection	224
8.3.5 MM-VB Dynamics Study of the Relative Stability of the Reverse Recoupling Species	228
8.3.6 Soliton Dynamics	231
a) short lifetime of the reverse recoupled species	232
b) long lifetime of the reverse recoupled species	234
c) normal recoupling (reverse recoupling is not involved)	235
8.4 Conclusion	248
Appendix 8 Supplementary Data	250

Chapter 9 Host-Guest Dynamics: Photoisomerisation within a Cyclodextrin Cavity	253-273
9.1 Introduction	253
9.2 Computational Details	256
a) Approximations	256
b) Z-matrix construction	257
c) Optimisation procedure	258
d) Other Details	259
9.3 Results and Discussion	260
9.4 Conclusion	270
Appendix 9 Supplementary Data	271
Chapter 10 Conclusion	274-276
References	277-283

Figures

1.1	General features found on the potential energy surfaces for a photochemical reaction.	18
1.2	Example trajectories illustrating dynamical behaviour over some typical features of a potential surface.	27
1.3	Diagram of an n -dimensional conical intersection.	29
1.4	Schematic potential surfaces for a reaction exhibiting a transition state leading to a conical intersection, and three ground state photoproducts.	31
1.5	3D and 2D representations of the three different types of conical intersection.	33
2.1	Illustration of the direct dynamics method, using a triatomic exchange reaction as an example.	36
2.2	The Landau-Zener hop probability.	57
2.3	Data from a benzene surface-hopping trajectory calculation.	61
2.4	The velocity vector is resolved into components parallel and perpendicular to the non-adiabatic coupling vector.	63
2.5	Arrangement of vectors after a surface hop.	65
2.6	The ‘ants’ method.	66
2.7	Diagram showing the method used for sampling the initial geometries.	68
2.8	The simple cloning scheme for computing the trajectory batches on an MPP machine.	71
2.9	Flowchart for the ‘driver’ program.	72
2.10	Flowchart for the ‘step’ program.	73
2.11	Screenshot from the main menu of TRAJIC.	75
3.1	MM-VB hybrid atom approach.	79
3.2	Schematic singlet (E_+) and triplet (E_-) potential curves of H_2 , showing their relation to the Coulomb (Q) and exchange (K) integrals.	82
3.3	The lowest energy conical intersection geometry for H_3 .	86
3.4	Effects included in the parametrisation of the two model systems.	90
3.5	Example MM-VB dynamics input for azulene.	96
3.6	Partial input decks for benzene, cyclohexadiene and octatetraene.	99
4.1	Azulene.	101
4.2	Azulene: a tipped conical intersection.	105
4.3	Comparison of MM-VB and <i>ab initio</i> energetics.	106
4.4	The geometrical transformation required to move from the Franck-Condon geometry to the S_1 minimum.	107

4.5	Plot of potential energy versus time for two azulene trajectories launched from the Franck-Condon region on S_1 with hopping disabled.	108
4.6	Plot of potential energy versus time for four typical surface-hopping trajectories. Three ‘snapshots’ from a trajectory are also shown.	111
4.7	Example of a reversible azulene trajectory with 150 steps and a trust radius of $0.048 \sqrt{\text{amu}}$ bohr.	115
4.8	Potential energy and kinetic energy for the forward trajectory of Figure 4.7. The sum PE+KE shows the conservation of energy.	116
5.1	S_1/S_0 photochemistry of benzene.	121
5.2	MM-VB optimised geometries for (a) planar S_0 minimum and (b) planar S_1 minimum.	123
5.3	MM-VB optimised conical intersection geometry.	124
5.4	Energy profile along the lowest frequency coordinate near the minimum energy point on the CI.	125
5.5	MM-VB geometry in the prefulvene region (not fully optimised).	126
5.6	Schematic representation of the S_1 and S_0 potential energy surfaces, showing the decay pathways to prefulvene and S_0 planar benzene.	127
5.7	MM-VB derivative coupling vector evaluated at the minimum energy point on the CI.	128
5.8	Initial energy distribution for two typical trajectory packets.	133
5.9	Analysis of batches with varying geometry sampling, showing standard deviations.	134
5.10	Plot of potential energy for an example benzene trajectory, together with ‘snapshots’ of the motion.	136
6.1	Summary of CHD excitation.	142
6.2	The three possible relaxation paths from the CHD conical intersection.	143
6.3	Illustration of the hypersphere method for locating initial relaxation directions (IRD).	146
6.4	Ground state steepest descent line generated from a point on the $0.025 \sqrt{\text{amu}}$ bohr radius circle located on the branching plane.	149
6.5	Surface hopping trajectory generated from a point on the $0.165 \sqrt{\text{amu}}$ bohr radius circle located on the branching plane.	149
6.6	MM-VB optimised conical intersection structure CI_{CHD} , derivative coupling vector x_1 , and gradient difference vector x_2 .	151
6.7	<i>Ab initio</i> optimised conical intersection structure CI_{CHD} , derivative coupling vector x_1 , and gradient difference vector x_2 .	152
6.8	Values of the C_1-C_6 and C_1-C_6 bond distances for the 20 points around the $0.025 \sqrt{\text{amu}}$ bohr radius circle.	153

6.9	Distribution of products based on the MM-VB steepest descent line results in Table 6.1.	154
6.10	Percentage yield for each packet of 64 surface hopping trajectories released from the branching space circle.	156
6.11	Schematic potential energy surfaces and reaction paths	158
7.1	Octatetraene Photoisomerisation.	163
7.2	Geometries of the S_0 all-trans and cis,trans isomers.	168
7.3	Geometry of the ‘adiabatic transition structure’ TS_{ad} .	169
7.4	Geometry of the ‘nonadiabatic’ transition structure TS_{nonad} .	169
7.5	Representation of the twisting motion required to pass through the nonadiabatic transition structure TS_{nonad} .	170
7.6	Geometry of the lowest energy point on the S_1/S_0 conical intersection.	171
7.7	(a) Gradient difference and (b) derivative coupling vectors for the lowest-energy point on the S_1/S_0 conical intersection.	173
7.8	(a) Potential energy and (b) isomerisation angle plotted as functions of time for trajectories launched from each side of TS_{ad} .	175
7.9	(a) Potential energy and (b) isomerisation angle plotted as functions of time for trajectories launched from each side of TS_{nonad} .	176
7.10	Energy profiles along the <i>ab initio</i> S_1 MEP connecting all-trans octatetraene to the S_1/S_0 crossing point.	179
7.11	(a) Potential energy and (b) dihedral angles plotted as functions of time for a trajectory launched from TS_{nonad} toward the all-trans minimum.	181
7.12	Snapshots taken from the trajectory plotted in Figure 7.11.	183
7.13	3D and 2D paths of trajectories launched from each side of TS_{nonad} .	185
7.14	Schematic potential energy surfaces as a function of the C_3-C_4 and C_5-C_6 dihedral angles.	187
7.15	Labelling of the trajectory batches.	190
7.16	Analysis of the 12 trajectory batches.	192
7.17	Analysis of batches with varying geometry sampling, also showing standard deviations.	195
7.18	3D and 2D paths of isomerising and non-isomerising trajectories.	197
7.19	Snapshots of geometries from the isomerising trajectory plotted in Figure 7.18.	198
7.20	Snapshots of geometries from the non-isomerising trajectory plotted in Figure 7.18.	199
7.21	Yield of cis-cis octatetraene.	200
8.1	Polyene chain and corresponding π -electron density wave..	210

8.2	(a) Symmetric double-well potential for an infinite-length polymer, and (b) non-symmetric double-well potential for a finite-length polyene.	210
8.3	General scheme for soliton propagation in a linear polymer or polyene.	212
8.4	The two recoupling pathways from the conical intersection, leading to 'reverse' and 'normal' polyene species.	214
8.5	MM-VB optimised ground state reverse recoupling minimum for octatetraene.	216
8.6	Stabilisation of the unpaired electrons by means of resonance structures.	216
8.7	Lifetimes of the reverse recoupling species for the 12 batches of excited state trajectories.	217
8.8	Number of trajectories in each batch which are still in the reverse recoupling state at the end of the simulation.	218
8.9	Chart showing where the longest and shortest reverse recoupling lifetimes are located with respect to the release angle.	218
8.10	MM-VB conical intersection geometry for hexatriene.	220
8.11	MM-VB conical intersection geometry for C ₁₂ H ₁₄ .	220
8.12	MM-VB ground state reverse recoupling geometry for tEt hexatriene (not fully optimised).	221
8.13	MM-VB optimised ground state reverse recoupling geometry for dodecahexaene (not fully optimised).	221
8.14	Ground state energetics for C ₆ H ₈ , C ₈ H ₁₀ and C ₁₂ H ₁₄ .	222
8.15	<i>Ab initio</i> evidence for reverse recoupling in tEt-hexatriene.	223
8.16	SDL paths from the branching plane circle for C ₁₂ H ₁₄ .	225
8.17	Plot of main bond lengths and geometries for a SDL path toward the reverse recoupling region in dodecahexaene.	227
8.18	C ₄ -C ₅ and C ₄ -C ₅ bond lengths for two randomly selected C ₁₂ C ₁₄ trajectories.	230
8.19	Snapshots from a trajectory with a short reverse-recoupling lifetime.	236
8.20	Snapshots from the same trajectory as 8.19, but viewed from the end of the chain.	238
8.21	Plot of main bond lengths for the trajectory shown in 8.19 and 8.20.	239
8.22	Exchange density data for the trajectory shown in 8.19 and 8.20.	240
8.23	Snapshots from a trajectory with a long reverse-recoupling lifetime	241
8.24	Exchange density data for the trajectory shown in 8.23	244
8.25	Snapshots from a trajectory following the 'normal' recoupling path.	245
8.26	Exchange density data for the trajectory shown in 8.25.	247
9.1	(a) A single glucopyranose unit. (b) α -cyclodextrin	253
9.2	Shape and dimensions of cyclodextrin.	254

9.3	The Z-matrix for the host-guest system.	258
9.4	The all-trans minimum geometry for the host-guest system.	261
9.5	The conical intersection geometry for the host-guest system.	263
9.6	The optimised excited state minimum and transition state structures superimposed to show the change in orientation within the cavity.	263
9.7	Main dihedral angles plotted as functions of time for the host-guest trajectory launched from TS_{nonad} toward the all-trans minimum.	264
9.8	Superimposed structures showing the twisting motion required to pass over the S_1 nonadiabatic transition structure.	265
9.9	Change in potential energy when stepping along the transition vector for the nonadiabatic transition state of (a) the isolated octatetraene system, and (b) the octatetraene-cyclodextrin system.	266
9.10	An example surface-hopping trajectory for the host-guest system.	268

Tables

5.1	Quantum yield of prefulvene as a function of excess energy along the reaction path.	130
5.2	Quantum yield of prefulvene as a function of excess energy in vibrational modes orthogonal to the reaction path.	132
6.1	Distribution of the 20 steepest descent lines released from evenly spaced points on the $0.025 \sqrt{\text{amu}}$ bohr radius branching plane circle.	154
7.1	Distribution of the 12 steepest descent lines released from evenly spaced points on a circle in the branching plane.	188
8.1	Time taken for the normal electronic recoupling is restored. Data obtained by analysing three batches of excited state trajectories.	229
9.1	Comparison of TS and CI geometries for the isolated and host-guest systems.	263

Acronyms

The following abbreviations are used:–

MD – molecular dynamics	PES – potential energy surface
PE – potential energy	KE – kinetic energy
CI – conical intersection	B-O – Born-Oppenheimer
F-C – Franck-Condon	L-Z – Landau-Zener
IC – internal conversion	ISC – intersystem crossing
MM – molecular mechanics	VB – valence bond
MEP – minimum energy path	IRC – intrinsic reaction coordinate
SDL – steepest descent line	IRD – initial relaxation direction
TSH – trajectory surface hopping	CHD – cyclohexadiene
HT – hexatriene	MCPD – methylenecyclopentene diradical
amu – atomic mass unit	RMS – root mean square
MC-SCF – multi-configuration self-consistent field	MPP – massively-parallel processing

Acknowledgements

I would like to take this opportunity to thank all those who have contributed to this work. Firstly, I would like to express my gratitude to Prof. Mike Robb for supervising me, and for all the help and guidance he has given over the years. I am also very grateful to Dr. Mike Bearpark for all those weeks of programming, and for his patience answering my many questions. I would also like to acknowledge Dr. Massimo Olivucci and Prof. Fernando Bernardi for their important contributions to this work and for the time I spent at the University of Bologna.

Thanks to Thom Vreven for all the surface-hopping discussions, and to Dr. Paolo Celani for his clear explanations of various aspects of theoretical chemistry and computing.

And to all the past and present theoretical chemists on the 8th floor — thanks for making it so much fun! Special mentions go to Maria Jesus Parrado, Merce Deumal, Dr. Paolo Celani (again) and Leticia Gonzalez for being such great friends to me.

I am also grateful to my reliable proof-readers, Alix Rickerby, Maria Jesus Parrado (again), and Dr Mike Bearpark (again), for hopefully finding most of my mistakes.

As always, I am indebted to my parents for all their support and encouragement. Thanks also to Dr. Dave Cross and Tony Gayler for their friendship and good advice over the years. I must also thank Prof. Manuela Merchan for being the most patient person on the entire planet.

Finally, I am grateful to King's College for a research studentship.

Chapter 1

Introduction

1.1 Modelling Photochemical Reactivity

Molecular dynamics (MD) [1, 2] is one of the most appealing ways to investigate a chemical reaction since it provides a series of step-by-step ‘snapshots’ of the atoms, allowing us to ‘see’ their journey from reactant to products. Given a set of initial positions for the atoms or molecules, the change in geometry at each successive step is found by solving equations of motion subject to a force field which contains the effect of the surrounding nuclei and electrons. The path taken by the system of atoms or molecules is the *trajectory*. A rigorous description of the electronic and nuclear motion is only obtainable by evolving the wavefunction by means of the time-dependent Schrödinger equation (see, for example, the wavepacket dynamics of Köppel *et al.* [3]), a problem which is a huge computational effort even for the smallest systems (currently, only two or three degrees of freedom can be included). Fortunately, classical mechanics, i.e. Newton’s second law, can describe the motion of the nuclei quite adequately in most situations, and the problem is greatly simplified.

The large disparity in velocity between the nuclei and electrons means that the two components can be separated via the Born-Oppenheimer approximation, discussed in detail later. This gives rise to the concept of a potential energy surface (PES) [4, 5], which is one of the most important tools for visualising reaction pathways and mechanisms. A PES is generated by mapping-out the electronic potential energy of the system as a

function of the various coordinates (degrees of freedom) describing the change in geometry of the nuclei. Minima on this surface correspond to the reactants and products (and sometimes intermediate structures). For a chemical reaction to occur there must be an energetically accessible pathway between the reactant and product minima. The minimum energy path (MEP) defines the route with lowest potential energy. In mass-weighted coordinates this is called the intrinsic reaction coordinate (IRC) [6]. If a high energy barrier lies somewhere along this path then the reaction may not occur at all. For a diatomic molecule there is only one internal degree of freedom (the bond length) and so the PES is simply a curve, but in general there are more than two geometric parameters to plot, and visualising the multi-dimensional surface (a *hypersurface*) is not so straightforward. A useful way to analyse the dynamics of a reaction is to consider the motion of a ball rolling on the potential energy surface. Each position of the ball corresponds to a unique geometry of the atoms. This is one of many ways of visualising the results of a trajectory calculation.

At this point we must make a distinction between a thermal reaction and a photochemical reaction. A thermal reaction is governed by the topology of a single potential energy surface (an *adiabatic* reaction), whereas a photochemical reaction starts with an excitation process [7], initiated by UV or visible light of the appropriate wavelength, transferring the system onto an *electronically excited state* [8]. More precisely, absorption of a photon by the singlet S_0 ground state produces an excited singlet state S_n . Intersystem crossing (ISC) can cause triplet states to be populated. Based on the Franck-Condon principle, which again relies on the fact that the electrons move much faster than the nuclei, the initial excitation is assumed to be a ‘vertical’ transition from a ground state minimum energy well, during which the nuclei have no time to adjust. The topology of the new potential surface then controls the dynamics of the nuclei, until ultimately the system decays back to the ground state. Hence, reactions which cannot occur thermally, due to prohibitively large energy barriers on the ground state potential surface, may become highly reactive via a photochemical mechanism.

The decay from the S_1 state back to the ground state can occur by fluorescence, or by internal conversion via a *radiationless* process. For many years the mechanism of decay without emission of radiation was not well understood. It was thought to occur at a minimum on the excited state, in a region of the potential where the ground and excited state surfaces become close at an avoided crossing. Such processes are slow, however, and fail to explain how systems could decay on a femtosecond timescale. More recently, it has been recognised that a true crossing of potential surfaces can take place, creating a new topological feature called a *conical intersection* (CI) (see [9, 10] and references therein). The intersection acts like a funnel linking the excited and ground state surfaces, providing a fully-efficient decay path back to the ground state products. There need not be a transition state separating the Frank-Condon region and CI, but if one is present it will control the conditions under which the radiationless route is accessible. Figure 1.1 summarises the general features found on a potential energy surfaces for a photochemical reaction. These ideas are explored further in Sections 1.2 and 1.3.

(See separate file for figure)

The idea that a conical intersection could play a key role in the decay mechanism for excited state reactions was proposed by Teller [11] more than 30 years ago. More recently, Zimmerman [12] and Michl [13] both suggested that the presence of a CI could be responsible for the specific photoproducts formed after transfer to the ground state via internal conversion. The literature now contains many theoretical studies of organic systems which find low-lying surface crossings — see the ‘highlight’ article by M. Klessinger [9], or for some recent examples see ref. [14]. Modern experimental techniques [15] have enabled researchers to verify the existence of conical intersections. Observing ultra-fast radiationless decay is the main indication of a mechanism involving a CI. Laser spectroscopy can now be performed at a sub-picosecond level, giving reliable data for excited state lifetimes, decay rates, and energy thresholds for these reactions. If the radiationless decay is thermally driven, i.e. it is ‘switched-on’ at a certain temperature [16], this suggests that a transition state lies on the excited state path leading to the intersection. Quantum yield measurements provide information about the product distribution, and hence the possible ground state paths accessible from the CI.

Currently, most theoretical studies of photochemical reactions in the literature rely solely on non-dynamical information to elucidate mechanistic information, i.e. structural analysis of critical points, intersections and minimum energy paths on the potential surfaces. Full-scale realistic dynamics simulations are usually considered too costly in terms of computer CPU time. The purpose of this thesis is to describe and implement a molecular dynamics method capable of accurately modelling the photochemistry of relatively large organic reactions without the need to neglect any degrees of freedom. In developing a method which is capable of achieving this goal there are three main aspects to consider:

- A method for computing classical trajectories efficiently.
- How to treat the system in regions where the classical approximation fails.
- Choice of force field for generating the potential energy surfaces and other data needed for the trajectories.

Each of these issues is discussed briefly below, and in detail in Chapters 2 and 3. The remaining sections in Chapter 1 introduce the Born-Oppenheimer approximation and potential energy surface.

Traditional techniques for computing classical trajectories are problematic when dealing with many degrees of freedom. One might usually expect to map-out the entire PES before starting a trajectory calculation, and use a piecewise or global fitting procedure to obtain usable functions (for example, see ref. [17]). *Direct dynamics* (Section 2.1), first formulated by Helgaker *et al.*[18], is a method which overcomes this problem by removing the need to compute the entire PES explicitly. Instead, the potential surface data is computed ‘on-the-fly’, as required by each specific trajectory.

In the vicinity of a conical intersection the Born-Oppenheimer approximation breaks down (see Section 1.2). The reaction is then described as *nonadiabatic*. By definition, classical trajectories are restricted to a single potential surface, and are not valid in regions where there is strong coupling between two or more electronic states. However, if the coupling region is localised then we can retain the classical trajectory model, but introduce a *semi-classical* algorithm to allow transfer of trajectories from one surface to another. Tully and Preston [19] were the first to suggest using trajectory surface hopping (TSH, Section 2.2) to model a nonadiabatic process.

Initial conditions for the simulations are controlled by a simple geometry sampling technique (Section 2.2.7). By computing a batch of trajectories we can follow the evolution of a ‘classical wavepacket’ over the potential surface. After analysing a number of these batches it is possible to gain valuable information about product yield distribution and other dynamic effects.

Computational details are discussed in Section 2.3, including flow-charts for the dynamics program, and an outline of how the code is implemented on a massively-parallel processing (MPP) computer. There is also a summary of the techniques used for analysing the results of individual trajectories and packets of trajectories.

The most time-consuming part of almost all MD simulations is the calculation of the force acting on each particle at every step. When studying photochemical systems one encounters a fundamental computational problem: the detailed bond-breaking / bond-making processes which occur in these reactions must be modelled by some form of quantum-mechanical potential. Ideally one would use an *ab initio* method, and there are many *ab initio* dynamics papers in the literature [20], but these are very costly. A typical trajectory calculation requires at least a few hundred steps, and moreover, to investigate a range of initial conditions may require many hundreds (or thousands) of individual trajectories, by which time *ab initio* quantum chemistry becomes far too inefficient. The solution is to employ a *hybrid* potential (Chapter 3), using a combination of quantum and classical theory to generate the electronic structure data required for the trajectory. One such method, MM-VB [21], combines molecular mechanics with valence bond theory, and is known to reproduce the essential features of ground and excited state potential surfaces for organic photochemical reactions. Using MM-VB and direct dynamics together [22] opens-up the possibility of investigating quite large systems (tens or hundreds of atoms) at relatively low computational cost, without neglecting any degrees of freedom in the simulation.

The remainder of the thesis documents applications of the method to a range of important photochemical reactions. The main aim is to examine the dynamical effects of reaction paths and to understand the factors controlling product distribution and quantum yields. Explaining the ultra-fast decay of azulene (Chapter 4) is a long-standing problem in photochemistry. However, the potential surface for this reaction is quite simple, and provides a good introductory system. It also highlights the fundamental role of the

conical intersection: the topology in the region of the surface crossing is directly responsible for the observed photochemistry. In Chapter 5, batches of trajectories ('classical wavepackets') are introduced to investigate the low quantum yield of prefulvene observed when benzene is irradiated. The interconversion of cyclohexadiene and hexatriene (Chapter 6) is a more subtle problem since in addition to the two major photoproducts there is the possibility of forming a third product. Again, packets of trajectories are used to explain the observed quantum yields. In particular, we look at the ground state pathways leading from the apex of the cone, and find that access to one of the photoproduct channels is severely limited. Our dynamics results for the *cis-trans* photoisomerisation of octatetraene (Chapter 7) confirm recent experimental findings, yet suggest that a highly complex reaction path is involved. Chapters 8 and 9 are of a more speculative nature, where we use MM-VB dynamics to predict photochemical behaviour for systems where little experimental or theoretical data is currently available. In Chapter 8 we show how the decay of linear polyenes via a conical intersection can produce highly intricate relaxation dynamics. On transfer from the excited state (S_1) to the ground state, polyenes are expected to perform an almost complete single/double bond reversal. However, electronic recoupling at the intersection can cause the 'wrong' recoupling to persist on the ground state surface. Dynamics results indicate that the lifetime of this meta-stable state increases for long-chain polyenes. Furthermore, coherent electronic and vibrational motions ('solitons') are observed during the recoupling phenomenon. Chapter 9 describes preliminary results of a dynamics study of an octatetraene molecule inside a cyclodextrin cavity. The restricted environment is found to cause a marked change in the dynamical behaviour of the excited octatetraene guest molecule. This final application chapter demonstrates the potential of MM-VB dynamics for studying host-guest systems and large organic systems in general.

Finally, Chapter 10 summarises the main results and observations which arise from this work.

1.2 The Born-Oppenheimer Approximation

The general form of the complete Hamiltonian operator (ignoring spin-orbit interactions) which governs the motion of a system of n electrons and N nuclei can be written as

$$\hat{H}_{tot} = T_{nuc}(\mathbf{R}) + \hat{H}_{el}, \quad (1.1)$$

where $T_{nuc}(\mathbf{R})$ is the kinetic energy operator for the nuclei (of mass M_I), which is a function of the nuclear geometry \mathbf{R} only,

$$T_{nuc}(\mathbf{R}) = -\frac{1}{2} \sum_{I=1}^N \frac{1}{M_I} \nabla_I^2. \quad (1.2)$$

\hat{H}_{el} is the electronic Hamiltonian, and is the sum of the remaining kinetic and potential energy operators (where \mathbf{r} represents the electronic coordinates, el =electronic, nuc =nuclear),

$$\hat{H}_{el} = T_{el}(\mathbf{r}) + V_{nuc-nuc}(\mathbf{R}) + V_{el-nuc}(\mathbf{r}, \mathbf{R}) + V_{el-el}(\mathbf{r}). \quad (1.3)$$

In atomic units, the expression becomes

$$\hat{H}_{el} = -\frac{1}{2} \sum_{i=1}^n \nabla_i^2 + \sum_{I < J}^N \frac{Z_I Z_J}{|R_I - R_J|} - \sum_{i=1}^n \sum_{I=1}^N \frac{Z_I}{|r_i - R_I|} + \sum_{i < j}^n \frac{1}{r_{ij}}, \quad (1.4)$$

where i and I are labels for the electrons and nuclei respectively, r is an electron-electron or electron-nuclear distance, R is a nucleus-nucleus distance, and Z is a nuclear charge.

The nuclei, being much heavier than the electrons, move relatively slowly which suggests that it would be reasonable to separate the two types of motion. This is the basis of the Born-Oppenheimer approximation (or separation). Rather than attempting to solve the Schrödinger equation in the space of all the variables, the nuclei can be considered as

fixed and the time-independent Schrödinger equation solved for the electrons alone (using the electronic Hamiltonian instead of the full Hamiltonian):

$$\hat{H}_{el}(\mathbf{r}; \mathbf{R}) \phi_k(\mathbf{r}; \mathbf{R}) = E_k(\mathbf{R}) \phi_k(\mathbf{r}; \mathbf{R}). \quad (1.5)$$

(from now on we drop the subscript and accent from \hat{H}_{el} , and assume we are always using the electronic Hamiltonian operator). The eigenvectors of this equation are the adiabatic electronic wavefunctions ϕ_k , which vary parametrically with nuclear configuration \mathbf{R} , but do not depend on the velocity of the nuclei. Consequently, we can write the total wavefunction $\Psi(\mathbf{r}, \mathbf{R})$ as the product of the electronic wavefunction $\phi_k(\mathbf{r}; \mathbf{R})$ and a nuclear wavefunction $\chi(\mathbf{R})$,

$$\Psi(\mathbf{r}, \mathbf{R}) = \phi_k(\mathbf{r}; \mathbf{R}) \chi(\mathbf{R}). \quad (1.6)$$

Solving Equation 1.6 for a particular nuclear geometry gives, in general, an infinite set of eigenvalues E_k . Moving in the configuration space \mathbf{R} then maps out the potential energy surface for each electronic state. The lowest energy solution gives the ground state surface. The other roots generate the excited state surfaces, although we might only be concerned with the lowest of these. The force acting on the nuclei at any geometry (for a particular potential surface) is simply obtained from the energy gradient,

$$F_I = -\frac{\partial E}{\partial \mathbf{R}_I}. \quad (1.7)$$

In most situations, the B-O approximation is reliable, but for one stage of a photochemical reaction it fails. When two potential surfaces are nearly degenerate, and the nuclear velocity is non-zero, nuclear and electronic motion become coupled, and the molecule no longer feels the effect of a single electronic state. The idea of a surface hop is then used as a way of dealing with this phenomenon in a semi-classical way, whilst still retaining the classical trajectory model. The mathematical details of trajectory surface hopping and nonadiabatic coupling are given in Section 2.2.

1.3 The Potential Energy Surface and its Interpretation

1.3.1 General Concepts

A molecule or group of molecules comprising N atoms will possess $3N-6$ degrees of freedom (or $3N-5$ in the case of a diatomic). These result from movement of each nucleus in three independent directions, but reducing this by six due to the three translations and rotations of the molecule as a whole, which leave the internal energy unchanged. Further degrees of freedom can sometimes be ignored if they correspond to small changes in potential energy. Thus, a PES can be constructed by plotting potential energy as a function of internal coordinates (or linear combinations of them) such as bond lengths or angles, $E(R_1, R_2, \dots, R_n)$. Such a plot is easily obtainable when only one coordinate is needed. However, even for a triatomic system we have $3 \times 3 - 6 = 3$ degrees of freedom, and thus four variables to plot. The PES must be constructed using a three-dimensional grid of points, each having an energy value $E(R_1, R_2, R_3)$. Multi-dimensional hypersurfaces are difficult to visualise but can be analysed using various graphical tools, such as isosurfaces (surfaces of constant energy). Often it is possible to reduce the problem to two important geometrical variables, and then plot the potential energy as a function of these alone. For a complex reaction, this approximation might not be meaningful, but it is still useful to draw a *schematic* potential surface, with reaction paths joining the critical points on the surface, even though the channels are multi-dimensional in reality. Information about the reaction mechanism and relative barrier heights can be successfully conveyed, and such diagrams are common in the literature.

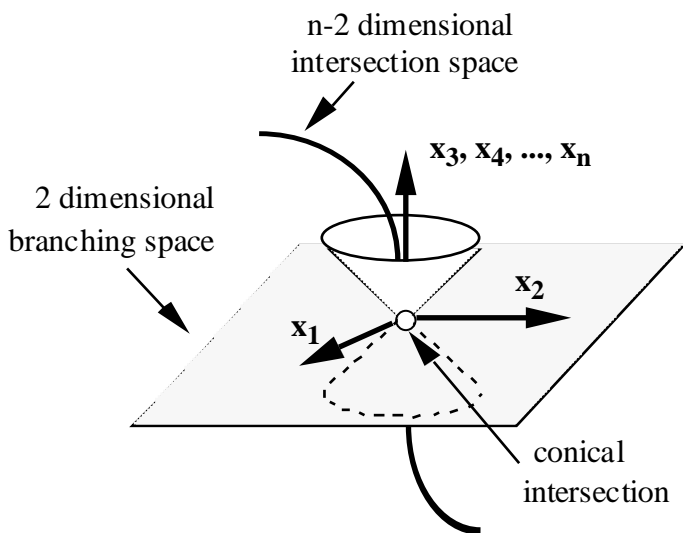
Features on the surface which are of chemical interest are the critical (fixed) points. At a critical point, the first derivative of the potential energy function with respect to all coordinates will be zero (i.e. $\partial E / \partial R_i = 0$, for all i). Minima occur if the second derivatives (the force constants) with respect to *all* coordinates are positive, and correspond to the stable products, reactants, or intermediate structures. Standard

optimisation (minimisation) techniques [23] are used to locate these points. Starting from a specified initial geometry, a Newton-Raphson-type formula uses the current first and second derivatives to compute a displacement (step) toward the local minimum. This is repeated until convergence, i.e. the forces and displacement become essentially zero. A saddle-point is found at transition structure geometries. Here, the surface is a maximum in the direction of the reaction path, and a minimum in the remaining directions. Higher order saddle points can exist, which have more than one direction of negative curvature. As an example of the dynamical behaviour which can occur on a potential surface, Figure 1.2 shows the results of two trajectories [24]. The first (Figure 1.2a) uses an analytic expression for a minimum, and shows how a trajectory can be trapped by the shape of the potential surface. Unless the trajectory is damped (i.e. kinetic energy removed) then it will continue to perform oscillations in the minimum. The second example (Figure 1.2b) shows the familiar potential surface for a linear triatomic exchange reaction (computed via a LEPS expression, see Section 3.3.2), to demonstrate a transition state between reactant and product valleys. If the trajectory has the correct magnitude *and* direction of momentum as it reaches the saddle point, then the barrier is surmounted and the reaction takes place. Although these appear to be rather simple examples, it turns out that dynamics over multi-dimensional surfaces can be understood in a very similar, intuitive way.

(See separate file for figure)

1.3.2 Conical Intersections

The preceding discussion focused on reactions governed by a single potential energy surface. Two potential surfaces can intersect along an $n-2$ dimensional hypersurface, where n is the number of independent variables in the potential function. It is easiest to begin by considering two potential energy curves, intersecting at a single point. Movement away from this point lifts the degeneracy. This idea can be extended to an arbitrary number of dimensions in the sense that we can always distinguish two vectors, say \mathbf{x}_1 and \mathbf{x}_2 (which are linear combinations of bond lengths, angles etc.), such that if one were to plot the energy as a function of these variables the surface would have the form of a double cone in the region of the degeneracy [25] (Figure 1.3). Hence the crossing is called a conical intersection (CI). More precisely, the branching plane is defined by the gradient difference and derivative coupling vectors, in Equation 1.8 and Equation 1.9 respectively, where we use the same notation as in the previous section. The derivative coupling (or nonadiabatic coupling) vector has a special significance when using a trajectory surface hopping algorithm since its magnitude and direction is a factor in determining where the hop occurs (Section 2.2). Any movement in the branching plane away from the intersection point will result in the degeneracy being lifted. Movement in the remaining $n-2$ dimensions (the intersection space) leaves the two surfaces degenerate, but may cause the potential energy to rise or fall.



$$\mathbf{x}_1 = \frac{\partial(E_1 - E_2)}{\partial \mathbf{R}} \quad (1.8)$$

$$\mathbf{x}_2 = \langle \phi_1 | \frac{1}{\partial \mathbf{R}} | \phi_2 \rangle \quad (1.9)$$

Figure 1.3 Diagram of an n -dimensional conical intersection.

In theory, trajectories can decay at any point on the intersection hyperline. However, if we assume that excited state trajectories will follow the lowest energy paths on the PES, then decay will most likely happen near the lowest energy point on the $n-2$ dimensional intersection space. As part of a systematic study of the potential surface for a photochemical reaction it is therefore normal practice to locate the minimum energy points on any surface crossings. This is achieved by requiring simultaneous convergence of two criteria [26]; the energy of the excited state surface is minimised in the $(n-2)$ -dimensional space orthogonal to \mathbf{x}_1 and \mathbf{x}_2 , and the energy difference $(E_1 - E_2)$ is minimised. Since \mathbf{x}_1 and \mathbf{x}_2 are the only two directions of motion with non-zero gradients, the initial ground state motion of a decaying trajectory must lie in the $\mathbf{x}_1 \mathbf{x}_2$ plane. Analysis of the geometric distortions caused by moving along \mathbf{x}_1 or \mathbf{x}_2 can provide clues as to which products will form. A number of criticisms can be applied to this approach. Firstly, trajectories are only likely to follow the minimum energy path under very low-energy (‘vibrationally cold’) conditions, such as those found in solution. Under gas phase conditions this will not be the case — trajectories may have large kinetic energy on the excited state surface. Moreover, under any conditions, decaying trajectories find themselves at the top of a ‘spike’ on the ground state potential. A conical intersection plays a fundamentally

different role to that of a transition state. A transition state lies on a reaction path connecting a *single* product minimum to a *single* reactant minimum, whilst a conical intersection can connect an excited state reactant with numerous ground state reaction paths and products. In fact, the normal definition of a reaction path — as the lowest energy route from reactants and products — is too simplistic to be applied to multi-surface reactions. Defining the reaction path through a conical intersection is a more subtle problem, to be tackled later (Chapter 6). Briefly, if the base of the cone is circular (as in Figure 1.3 above) then all directions of decay are equally likely (neglecting the momentum carried from the excited state). However, if the base of the cone is elliptic then two sides automatically become more favourable paths for trajectories. More generally, a number of decay paths may exist at the apex of the cone, and others may develop further down the manifold, all influencing product formation. Prediction of photoproduct distribution depends on this topology, coupled with the effects caused by the kinetic energy possessed by the trajectories. Large amounts of kinetic energy can be gained on the ground state surface, and take trajectories far from the minimum energy paths. Hence, there are many reasons for wanting to obtain both dynamical and structural information for reactions involving conical intersections. Figure 1.4 illustrates a schematic potential surface for a reaction exhibiting a transition state leading to a conical intersection, and three ground state photoproducts.

(See separate file for figure)

So far we have only seen situations where the apex of the cone is locally the lowest energy point on the excited state surface, and the highest energy point on the ground state surface. This is called a *peaked* conical intersection. In fact there are three types of intersection, each influencing the dynamics in a different way. The distinction between these is shown in Figure 1.5. When viewing the peaked CI in two dimensions (Figure 1.5a) it is clear that the two intersecting curves have gradients of opposite sign. However, if the curves have gradients of the same sign (Figure 1.5c) then the lowest energy point on the intersection lies above the local minimum — the conical intersection is *tipped* (or *sloped*). The *intermediate* case is shown in Figure 1.5b. Here, the excited state part of the surface is almost flat in the region of the intersection, and one curve has a near-zero gradient. The terminology used is that of Ruedenberg *et al.* [27]. Later we shall see examples of all three shapes of conical intersection, and find that the surface topology is a critical factor governing the formation of photoproducts.

(See separate file for figure)